JGR Atmospheres

RESEARCH ARTICLE
10.1029/2025JD044393

Special Collection:
Quantifying Nature-based Climate Solutions

Clustered Land Restoration Projects Increase Cloud Formation in West African Drylands

J. Ruijsch[2], A. J. Teuling[3], C. M. Taylor[4,5], G. J. Steeneveld[6], and R. W. A. Hutjes[1]

[1]Earth Systems and Global Change Group, Wageningen University and Research, Wageningen, The Netherlands, [2]Hydro-Climate Extremes Lab (H-CEL), Ghent University, Ghent, Belgium, [3]Hydro-Climate Extremes Lab (H-CEL), Ghent University, Ghent, Belgium, [4]UK Centre for Ecology and Hydrology, Wallingford, UK, [5]National Centre for Earth Observation, Wallingford, UK, [6]Meteorology and Air Quality Group, Wageningen University and Research, Wageningen, The Netherlands

Abstract Land restoration projects are implemented across Africa to combat land degradation and climate change. By changing the vegetation cover, these projects can potentially impact cloud formation through changes in energy and water partitioning between the Earth's surface and the atmosphere. In West Africa, satellite observations have shown an increase in cloud formation over restored areas. However, even though the spatial arrangement of restored areas differs between regreening approaches, such as farmer-managed natural regeneration, area protection or reforestation, it is unknown how the spatial pattern of restoration projects impacts cloud formation. In this study, we use the Weather Research and Forecasting (WRF) mesoscale atmospheric model to determine how land restoration affects cloud formation for a case study at the border of the transnational W-Arly-Pendjari national park complex, with a sharp boundary between forest and grassland. First, we carry out a sensitivity analysis to determine the underlying mechanisms of cloud formation over forest regions, after which we run 27 land restoration scenarios with low (21%), intermediate (43%), and high (85%) forest cover and varying spatial clustering to assess the impact of land restoration patterns on cloud formation. The results highlight that an intermediate forest cover with higher clustering increases cloud formation due to stronger mesoscale circulation. A small scale heterogeneity in forest cover or a high forest cover, on the other hand, inhibits cloud formation. Because clouds play an important role in the Earth's water and energy balance, these results provide important insight into how projects can be designed to increase their climate benefits.

Plain Language Summary In Africa, many land restoration projects aim to fight land degradation and climate change, often increasing vegetation cover in the restored area. This change in vegetation affects cloud formation by altering the exchange of water and energy between land and atmosphere. Earlier studies found that more vegetation usually leads to more clouds. But we still do not know if the way restored areas are arranged—whether forests are clumped together or spread out—matters for cloud formation. In this study, we used the Weather Research and Forecasting weather model to explore this question in a region at the edge of the W-Arly-Pendjari national park in West Africa. This area has a clear divide between forest and grassland. We simulated scenarios with different surface characteristics to study how forests influence cloud formation and scenarios with different amounts and patterns of forest cover. We found that more clouds form when forests are grouped together in large patches. This is because the large patches of forest create strong mesoscale circulations that enhance cloud formation. This shows that the pattern in which restoration projects are implemented can influence cloud formation. Designing land restoration projects with this in mind can, therefore, help maximize the climate benefits of these projects.

Key Points:

- Enhancing soil moisture suppresses cloud development over forests, whereas increased surface roughness and reduced albedo facilitate it
- Clustered large-scale restoration increases cloud formation compared to heterogeneous small-scale restoration due to mesoscale circulation
- Increasing forest cover can locally reduce cloud formation due to reduced large-scale heterogeneities

Supporting Information:

Supporting Information may be found in the online version of this article.

Correspondence to:

J. Ruijsch,
jessica.ruijsch@ugent.be

Citation:

Ruijsch, J., Teuling, A. J., Taylor, C. M., Steeneveld, G. J., & Hutjes, R. W. A. (2026). Clustered land restoration projects increase cloud formation in West African drylands. *Journal of Geophysical Research: Atmospheres*, *131*, e2025JD044393. https://doi.org/10.1029/2025JD044393

Received 23 MAY 2025
Accepted 24 DEC 2025

1. Introduction

Land restoration is seen as a promising solution to combat land degradation and climate change through carbon sequestration (Cook-Patton et al., 2020; Roe et al., 2019), while it simultaneously provides ecosystem services such as wood, food, shade and income when implemented in the right way (Holl & Brancalion, 2020). In West African drylands, which are especially vulnerable to land degradation and climate change (Prăvălie, 2021), many countries have pledged to restore land (PBL, 2020) or implement restoration projects under the current United Nations Decade of Ecosystem Restoration (UNEP, 2021). These projects aim to restore vast areas of land to mitigate climate change, enhance biodiversity and combat land degradation (Martin et al., 2021) and include, for

example, natural regeneration, area protection, farmer-managed natural regeneration, or active reforestation (tree planting).

In addition to climate change mitigation through carbon sequestration, land restoration also directly impacts the local climate through biophysical processes. Regions with a high vegetation cover often have a higher aerodynamic roughness, lower albedo, and transpire more water than nearby regions with a lower vegetation cover, increasing energy and water exchange between the Earth's surface and the atmosphere (Bonan, 2008; Duveiller et al., 2018; Hoek van Dijke et al., 2022). On a local scale, the increased evaporation often has a cooling effect on the restored area (Feldman et al., 2022; Ruijsch et al., 2024; Zhang et al., 2024), which can provide comfort for the local population (Vancutsem et al., 2010; Wolff et al., 2018). However, globally, the decreased albedo of restored areas will increase surface temperatures. This so-called albedo warming is increasingly being acknowledged when implementing land restoration projects (Hasler et al., 2024; Kirschbaum et al., 2024; Kristensen et al., 2024; Windisch et al., 2021).

In addition to temperature, land restoration can also impact boundary layer development and cloud formation through land-atmosphere interaction. Regions with a high vegetation cover (e.g., forests) often have a low albedo, which results in a higher amount of available energy at the surface. Combined with a high aerodynamic roughness, this provides the heat and turbulence necessary for daytime boundary layer growth. In addition, a relatively high evapotranspiration adds moisture to the atmosphere and lowers the lifting condensation level (LCL) and level of free convection. This combination of available energy and moisture can result in enhanced cloud formation over areas with a high vegetation cover (Bosman et al., 2019; Teuling et al., 2017). However, the enhanced evapotranspiration over vegetated areas also increases the allocation of available energy to the latent heat flux, at the expense of the sensible heat flux. This reduces boundary layer growth and can, in some cases, result in reduced cloud formation over vegetated areas compared to nearby sparsely vegetated regions. For example, although temperate and boreal forests in Europe, Asia and North America often show cloud enhancement, tropical forests in the Amazon and Central Africa sometimes inhibit cloud formation (Xu et al., 2022). These regions with enhanced cloud formation correspond to regions where the forest has a higher sensible heat flux compared to reference regions, assuming there is enough water vapor present in the atmosphere to condense (Taylor, Klein, Parker, et al., 2022; Xu et al., 2022).

However, the impact of vegetation on cloud formation also depends on its surroundings. If a forest borders sparsely vegetated areas, the differences in temperature and surface roughness can trigger thermally or dynamically driven mesoscale circulation and convergence (Birch et al., 2014; Garcia-Carreras et al., 2010; Spracklen et al., 2018), which are sometimes referred to as forest-breezes. Whether clouds form over the restored region, or the surrounding regions with lower vegetation cover, depends on whether the restored region is relatively cold (due to increased evapotranspiration) or warm (due to the decreased albedo). In addition, the effect of forests on cloud formation can vary through time (Qin et al., 2025). Similarly, if evapotranspiration is limited by soil moisture, dry conditions result in a higher allocation of net radiation toward the sensible heat flux, increasing surface temperature (Miralles et al., 2012) and boundary layer development (Ek & Holtslag, 2004; Findell & Eltahir, 2003). Through changes in the surface energy balance, soil moisture anomalies and gradients can impact convection, mesoscale circulations and precipitation (Klein & Taylor, 2020; Taylor, 2015; Taylor et al., 2007, 2012; Westra et al., 2012). This important role of vegetation in cloud formation is often overlooked when restoration projects are implemented, as the complex interaction of these processes makes it difficult to predict how restoration will impact cloud formation in a particular region (Lawrence et al., 2022).

In West Africa, satellite observations have shown enhanced cloud formation over restored areas (Ruijsch, Taylor, et al., 2025). However, the existence of mesoscale circulation, convergence and forest-breezes suggests that the spatial context of land restoration projects is an important factor determining cloud enhancement. Cloud enhancement has been, for example, observed only over project areas larger than roughly 10 by 10 km (Ruijsch, Taylor, et al., 2025). In addition, previous research shows that simultaneously increasing tree heterogeneity and tree cover enhances cloud formation in Africa by 55.2% compared to a uniform increase in tree cover (Xie et al., 2025). Idealized land cover simulations show that sharp land cover boundaries initiate convective initiation at the land cover boundaries (Ascher et al., 2025), depending on the scale of the heterogeneities (F. Chen & Avissar, 1994; Lynn et al., 1998). Yet, it remains unknown how (realistic) spatial patterns in which the land restoration projects are implemented influence cloud formation, even though different types of land restoration projects may result in considerably different spatial patterns of vegetation. For example, farmer-managed natural

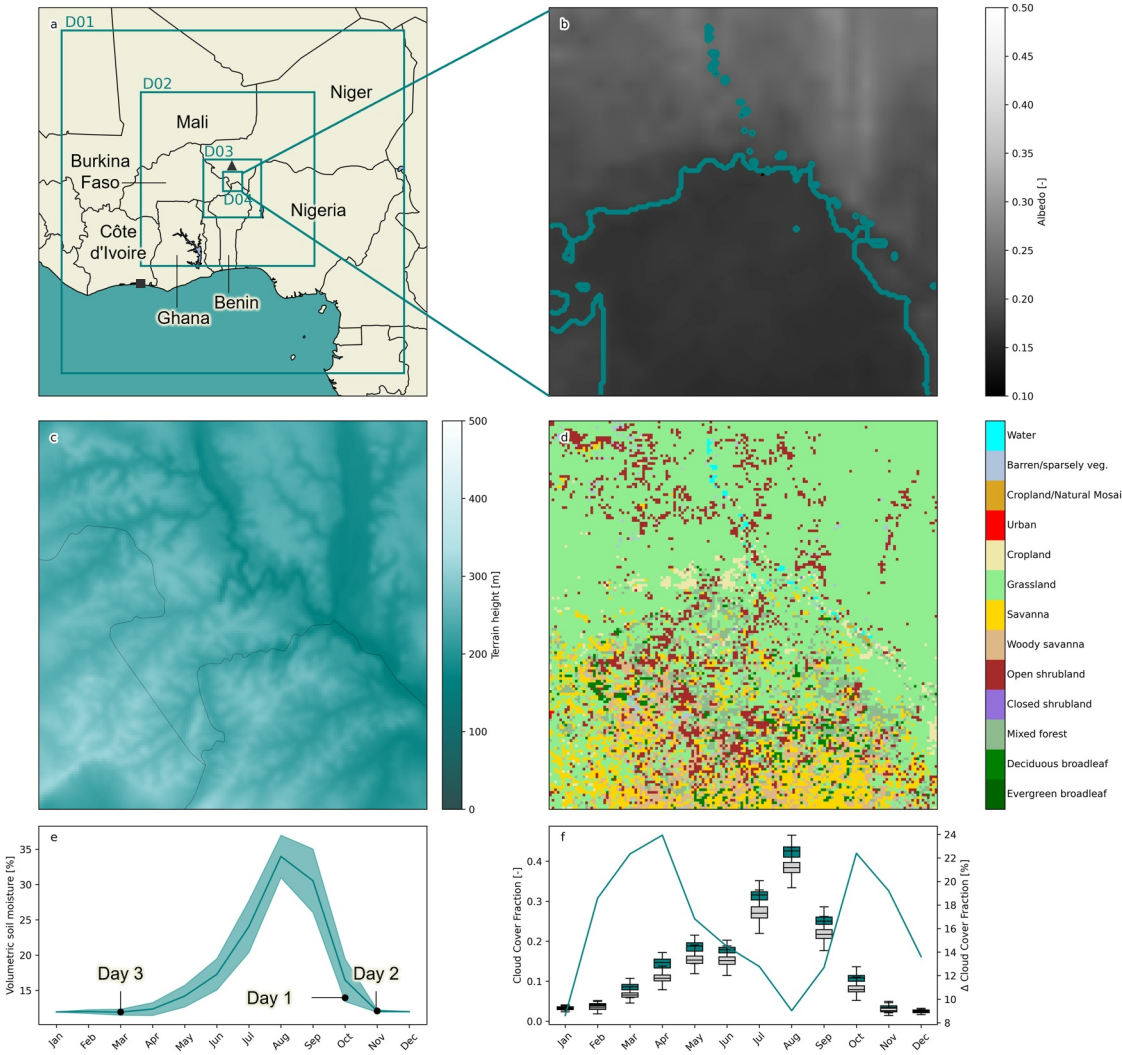

Figure 1. Study area and period. (a) Weather Research and Forecasting model domains and validation locations in Niamey (gray triangle) and Abidjan (gray square). (b) MODIS albedo on 1 October 2017 in domain 4. The line indicates the edge of the forest region. (c) Topography and (d) MODIS land cover as used in the model in Domain 4. Climatology of soil moisture content from ERA-5 and soil moisture on the three case study days (dots). (f) Climatology of cloud cover fraction in the forested (blue boxes) and grassland (gray boxes) area. The line shows the relative difference in cloud cover fraction between those two regions. Data in this panel is obtained from (Ruijsch, Taylor, et al., 2025).

regeneration is expected to result in smaller patches (at the scale of several trees) of vegetation within an agricultural or grassland region. Protected areas or active reforestation, on the other hand, will create large, continuous patches of vegetation (at the scale of tens of square kilometers).

This research aims to close this gap by determining how the spatial pattern in which land restoration projects are implemented affects cloud formation in West African drylands. However, the many factors impacting cloud formation result in noisy signals, which would make it difficult to extract relations from observation data alone. On top of that, the limited flux measurements make it challenging to determine underlying cloud development mechanisms. To this end, we use the Weather Research and Forecasting (WRF) model (Skamarock et al., 2019) to simulate cloud formation in West Africa. First, we run the model with the current vegetation cover over a study region with a sharp boundary between forest and non-forest (Figure 1) to determine how different surface characteristics (i.e., albedo, surface roughness and soil moisture) affect cloud formation. Even though land restoration can encompass a wide range of measures, we compare a forested protected area to a surrounding grassland area as a proxy for the potential effects of land restoration on cloud formation. Using this knowledge,

Table 1
Characteristics of the Model Domains

Domain	Number of grid cells	Domain size (km)	Grid cell size (km)	Domain latitude and longitude (NW, SE)	Time step (day 1 and day 2, day 3) (s)
D01	100 × 100	2,700 × 2,700	27	(22.683, −10.259), (−1.165, 14.260)	162, 100
D02	151 × 151	1,359 × 1,359	9	(18.556, −4.230), (6.458, 8.226)	32.4, 20.0
D03	151 × 151	453 × 453	3	(13.946, 0.376), (9.901, 4.513)	6.48, 4.00
D04	151 × 151	151 × 151	1	(13.090, 1.794), (11.741, 3.175)	1.30, 0.80

Note. Domain name, number of horizontal and vertical grid cells, domain size, grid cell size, and coordinates of the model domains.

we simulate several realistic land restoration scenarios with varying forest extent and spatial clustering to determine how the spatial pattern of land restoration affects cloud formation.

Our results can inform land restoration projects on how their project design may impact cloud formation through changes in vegetation cover. Ultimately, this may lead to the optimization of project design to obtain maximum climate benefits. Clouds provide shade and play an important role in initiating convective rainfall in the Sahel (Mathon et al., 2002), through which land restoration can impact water availability on a larger scale (Hoek van Dijke et al., 2022; Te Wierik et al., 2024). This may be needed to sustain restoration projects in dryland regions. At the same time, clouds impact the energy balance of the Earth and have the potential to impact global climate patterns (Goessling et al., 2025), both through trapping heat emitted by the Earth's surface and reflecting incoming solar radiation. Determining the impact of land restoration on cloud formation is, therefore, a crucial next step to form a more complete understanding of the overall climate effect of land restoration.

2. Materials and Methods

2.1. Case Study Description

We focus on a study region in West Africa. The region of interest is 150 by 150 km and located on the northernmost edge of the W-Arly-Pendjari Complex, a transnational protected area on the borders of Benin, Niger and Burkina Faso (11.7–13.1°N, 1.8–3.2°E) (Figure 1a). This case study area was selected because the border of the protected area shows a clear boundary in land cover and albedo (Figure 1b) and limited elevation differences (Figure 1c). The region inside the protected area mainly consists of natural vegetation types like savanna, shrublands and mixed forest, whereas the outside region largely consists of grassland (Figure 1d). Satellite observations between 2004 and 2024 show a structurally higher cloud cover fraction over the protected area compared to the surrounding region, with large relative differences at the start and end of the wet season (Figure 1f) (Ruijsch, Taylor, et al., 2025). To meet computational constraints, we selected three case study days referred to as Day 1 (1 October 2017) Day 2 (5 November 2004) and Day 3 (24 March 2013) (Figure 1e). These days were selected because satellite observations show a particularly high difference in cloud cover fraction over the forested area compared to the grassland area, based on data from Ruijsch, Taylor, et al. (2025), ensuring a day with land-atmosphere coupling and a potential effect of the forest cover on cloud formation. The case study days are ahead and following the wet season (Figure 1e) with a light wind (roughly 5 knots) is coming from the southwest (Figures S1a–S1f in Supporting Information S1). In addition, the soil moisture content in the southwest and southeast of the domain is relatively high compared to the forested area and the northeast grassland area (Figures S1g–S1i in Supporting Information S1). On Day 2, the soil moisture content is more homogeneous across Domain 4.

2.2. Model Description and Configuration

The (Advanced Research) Weather Research and Forecasting model (WRF-ARW) version 4.1.4 is run for the three case study days with four nested model domains (Figure 1a) with decreasing grid sizes of 27 km in the largest domain and 1 km in the smallest domain (Table 1). The initial and boundary conditions, including soil moisture, are provided by the European Center for Medium-Range Weather Forecasts (ECMWF) operational analysis with a 0.25 spatial grid length and a 6-hr temporal resolution. The model albedo, land use classes and leaf area index values are based on MODIS climatology data (Broxton et al., 2014), with a 1 km grid length in the

smallest domain. The surface roughness is based on tabled data linked to the land use class (Table S2 in Supporting Information S1).

In the two largest domains, cumulus development is parameterized using the Grell-Freitas ensemble scheme, while in the smallest domains, the spatial grid length (1–3 km) is low enough to assume that the cumulus development is resolved. In addition, we used the YSU scheme for the boundary layer (Hong et al., 2006), the Revised MM5 Monin-Obukhov scheme for the surface layer (Grell et al., 1994), the Unified Noah land-surface model for the land surface (S. Chen et al., 2022), the WSM 6-class graupel scheme for microphysics (Hong & Lim, 2006) and the rrtmg scheme for shortwave and longwave radiation (Oreopoulos & Barker, 1999). These parameterizations are considered suitable for answering the research questions (Achugbu et al., 2020; Klein et al., 2015). The start of the simulation was set to 00:00 UTC one day prior to the selected day to allow for adequate spinup (Jankov et al., 2007; Kleczek et al., 2014), and run until 23:59 UTC the next day, resulting in a simulation period of 48 hr. The model top is set to 3,000 Pa, with 8 levels in the lowest 1 km. For Day 1 and Day 2, the model is run with a timestep of 162 s (in Domain 1) and 61 vertical levels. To avoid numerical instabilities, Day 3 is run with a timestep of 100 s and 81 vertical levels. Output data is provided on a 15-min temporal resolution.

2.3. Model Evaluation

The model results are evaluated against multiple sources. We used radiosonde measurements from the University of Wyoming Upper Air Sounding Data Set (University of Wyoming, 2025) to evaluate vertical profiles of potential temperature, temperature, wind speed and wind direction. Because soundings are limited in Africa, no soundings were available in Domain 4. To this end, we compared model results in Domain 3 and Domain 1 with radiosonde measurements in, respectively, Niamey, Niger (13.48°N, 2.16°E) and Abidjan, Côte d'Ivoire (5.25°N, 3.93°W) (Figure 1a). The soundings are available for the three case study days at 12:00 UTC, except on 5 November 2004, where data were only available in Niamey.

To evaluate the modeled cloud formation, we use cloud masks derived from the High Resolution Visible band of the SEVIRI sensor onboard the Meteosat Second Generation Satellites (Ruijsch, Taylor, et al., 2025). Because we are interested in cloud formation over forest and grassland areas, we separate the study area into a "forest" area and a "grassland" area. The forest area is defined as having an observed mean albedo lower than 0.175 on 1 October 2017, based on Broxton et al. (2014), similar to the forest area in Ruijsch, Taylor, et al. (2025) and visibly matching the land cover boundary and protected area (Figure 1b). Although the forest area does not only contains forest, but mix of deciduous broadleaf forest (5.0%), mixed forest (13.6%), open shrubland (12.7%), woody savanna (13.9%), savanna (18.8%), and grassland (32.9%), it is referred to "forest" for convenience. The grassland area is the remaining part of the domain and consists mainly of grassland (85.8%) and open shrubland (8.6%) (Figure S4 in Supporting Information S1). The same forest boundary is used for all case study days to ensure similarity between seasons. Since cloud masks are not directly provided by the WRF model outputs, we defined a cloud mask based on locations where the liquid water path in the vertical column exceeds 1 mm (1,000 g/m^2) based on visual inspection of cloud patterns (Figures S2 and S3 in Supporting Information S1). The fractional cloud cover can then be defined as the fraction of clouds compared to the total area (the forest area, the grassland area or across the entire domain). The cloud cover fraction development over the forest and grassland area during the case study days is then compared to the cloud cover fraction observed with the satellite data. We compared the observed cloud cover fraction to the simulated cloud cover fraction in Domain 4 between 11.7°N and 13.0°N.

2.4. Sensitivity Analysis

To provide more insight into underlying relations between forests and cloud development, we carried out a sensitivity analysis by varying the albedo, surface roughness and soil moisture, all of which are expected to impact cloud formation. The parameters are varied over the forest area only, by multiplying the reference value (listed in Table S1 in Supporting Information S1) provided by the MODIS and ECMWF operational analysis data with a certain multiplication factor. Each parameter changed in three steps, resulting in 27 parameter combinations (Figure S5 in Supporting Information S1). The albedo is decreased (with multiplication factors of 1.0, 0.75, and 0.5), and the surface roughness and soil moisture content are increased (with multiplication factors of 1.0, 1.5, and 2.0) relative to the grassland, as these are typical surface characteristics through which forests are hypothesized to impact cloud formation (e.g., Xu et al., 2022).

The albedo is changed within Domain 4 only. The soil moisture is changed in both Domain 4 and 3 across all vertical layers to avoid strong soil moisture discontinuities. Because the surface roughness is based on tabled data linked to the land use class, we multiply the minimum and maximum roughness length (Z0min, Z0max) for the evergreen broadleaf forests, deciduous needleleaf forests, deciduous broadleaf forests, mixed forests, closed shrublands, woody savannas, savannas, and croplands classes across the model domain. To study the effect of these parameters on cloud formation, we determined for each time step the cloud cover fraction over the forest and grassland areas. In addition, to provide more insight into the underlying processes, we retrieve other variables such as the sensible heat flux, latent heat flux, planetary boundary layer height, LCL and vertical wind profiles. The planetary boundary layer height is defined as the lowest height where the bulk Richardson number exceeds the critical threshold (in this case, 0.25).

2.5. Restoration Scenarios

To determine the effect of forest size and heterogeneity on cloud formation, we created different restoration scenarios with varying land cover patterns. To reduce the number of variables, we only used the "grassland" and "mixed forest" (which has albedo and roughness values in-between the other land cover types, Table S2 in Supporting Information S1) MODIS land covers. We created random patterns with varying forest cover and spatial clustering, following Lennon (2000), generating two-dimensional random patterns similar to patterns found in natural systems. In total, we created 27 restoration scenarios, using combinations of three forest covers values: 21.3% (half of the reference forest cover), 42.7% (the reference forest cover) and 85.4% (two times the reference forest cover). In addition, we used three so-called dispersion values that represent the degree of spatial clustering (−1.0, −2.5, and −5.0), and three random variations (seed 1, seed 2, and seed 3) (Figure S6 in Supporting Information S1). A detailed description of the generation of these patterns is given in Text S1 in Supporting Information S1. In addition, we simulated a scenario with only grassland and only mixed forest for comparison.

The land cover scenarios were simulated for one of the case study days (1 October 2017) with a similar model configuration as in the reference simulation. However, in order to determine how forest pattern impacts cloud formation, we create conditions where we expect cloud development over the forest (as observations show for this case study day). Based on the results of the sensitivity analysis (e.g., cloud formation over soil moisture boundaries) and existing literature (Taylor et al., 2011), we expect soil moisture heterogeneities be an important factor determining cloud formation over forests. Therefore, we used the domain average soil moisture in the grassland regions, and half the domain average in the forest. Based on these model simulations, we compared cloud development over forest and grassland areas in the same way as for the sensitivity analysis.

3. Results

3.1. Evaluation of Model Results

To validate the model results, we compared the reference model simulation with radiosonde measurements. On Day 1, the simulated height profiles (represented by air pressure) of temperature closely follow the measurements at Niamey (13.48°N, 2.16°E) (Figure 2a). However, near the surface (1,000–800 hPa), the simulated dew point temperature is up to 9.3°C lower than measured values, suggesting the model simulates a drier boundary layer, resulting in a higher simulated LCL (153.2 hPa). Also at a higher level, between 600 and 300 hPa, the dew point temperature is underestimated. The simulated Convective Available Potential Energy (CAPE) is lower (675.7 J/kg) than the measured value (3,101.8 J/kg), while no Convective Inhibition (CIN) is simulated, but a value of −56.76 J/kg is measured. On Day 2, simulations of dew point temperature are underestimated at the surface (1,000–900 hPa), and the simulated LCL is 75.0 hPa higher than the measured value (Figure 2b). Both the measured and observed CAPE and CIN have a value of 0.0 J/kg. On Day 3, a similar pattern is observed, with an underestimation of dew point temperature (10.3°C) between 1,000 and 900 hPa and a higher simulated LCL (127.9 hPa) (Figure 2c). On this case study day, the model simulated a CAPE and CIN of 0.0 J/kg, while the measured values are 171.7g and −191.0 J/kg, respectively. So, during all three case study days, the simulated LCL is lower than the observed value due to a dry simulated boundary layer, although these local humidity biases due to soil moisture anomalies are not unusual to occur in the Sahel (Taylor et al., 2007). In Abidjan (5.25°N, 3.93°W), the simulations follow the measurements more closely on Day 2 and Day 3, both in terms of the LCL as the dew point temperature near the surface (Figure S7 in Supporting Information S1).

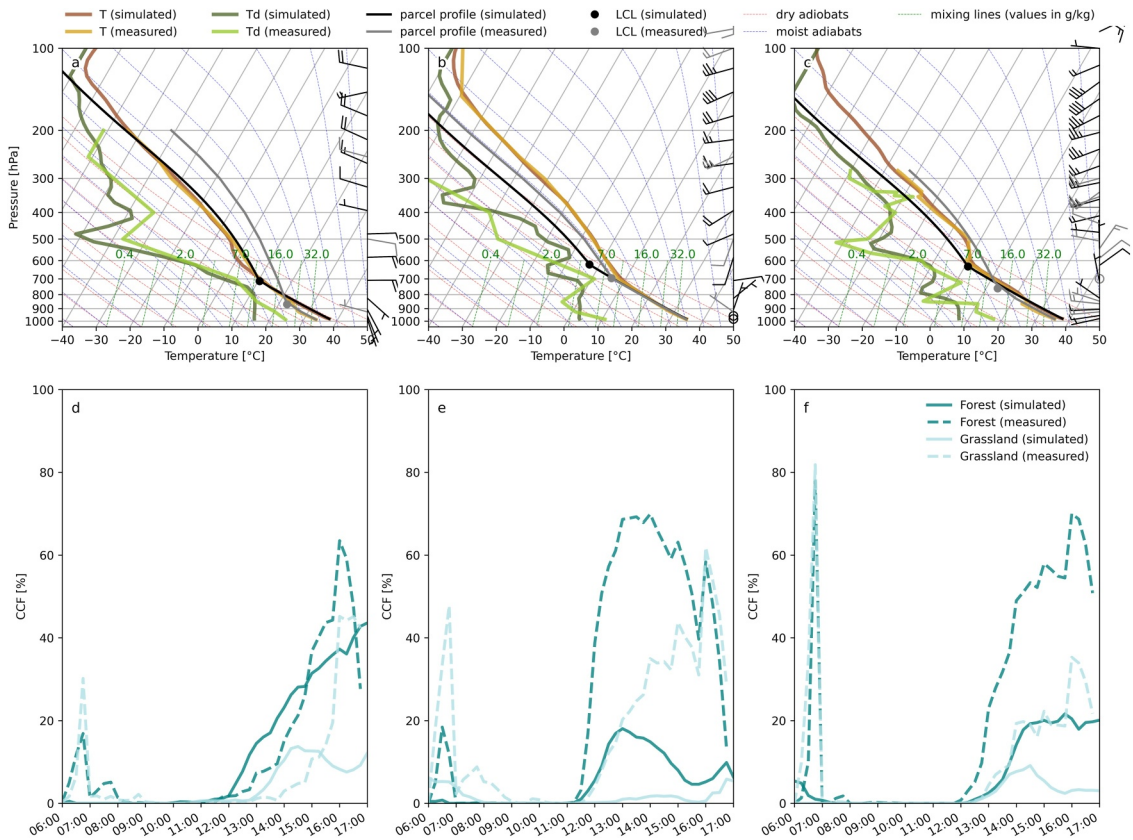

Figure 2. Evaluation of model results. Thermodynamic diagram of simulated (Weather Research and Forecasting) and measured (sounding) temperature (*T*), dew point temperature (Td), parcel profile, lifting condensation level and wind speed and direction (barbs, simulated is black, measured is gray) at Niamey on Day 1 (a), Day 2 (b), and Day 3 (c). Simulated temperature, dew point temperature and pressure are obtained from Domain 3 at the location of Niamey. Simulated and measured cloud cover fraction inside and outside the forest on Day 1 (d), Day 2 (e), and Day 3 (f) in Domain 4.

In addition, we evaluated simulations of cloud cover with satellite observations. Although the simulated cloud cover fraction inside the forest region on Day 1 is underestimated during the beginning of the afternoon and overestimated after around 15:00, the simulated development of the clouds follows the pattern of measurements (Root Mean Squared Error (RMSE) = 6.0%, maximum bias ($bias_{max}$) = 16.7%, between 06:00 and 16:45 UTC). Outside the forest, the model predicts a lower cloud cover than the observations, especially at the end of the afternoon (RMSE = 9.9%, $bias_{max}$ = 37.0%) (Figure 2d). On Day 2, the cloud cover is underestimated by the model, both inside (RMSE = 28.9%, $bias_{max}$ = 55.1%) and outside (RMSE = 18.7%, $bias_{max}$ = 42.8%) the forest, compared to observations, but follows a similar onset of cloud development to the observations (Figure 2e). On Day 3, the simulated cloud cover is overestimated as well, both inside (RMSE = 21.1%, $bias_{max}$ = 76.9%) and outside (RMSE = 15.8%, $bias_{max}$ = 81.8%) the forest (Figure 2f). In addition, the onset of cloud development has a similar timing, although the similar cloud cover outside the forest decreases after 15:00, which is not observed from the satellite data. So, the model simulates a lower cloud cover fraction than observational data, especially on Day 2 and Day 3. Although a direct verification of the reason for this underestimation is challenging due to the limited data availability in the smallest domain, this bias could be linked to the too dry boundary layer and too high lifting condensation as observed in the sounding data. Nonetheless, across all three case study days, both the model simulations and the measurements indicate a higher cloud cover over the forest area than the surrounding non-forest area, which justifies the use of this model configuration for studying mechanisms for enhanced cloud formation over the forested area.

3.2. Relationship Between Vegetation Characteristics and Cloud Formation

In this subsection, we will discuss results in our area of interest (Domain 4) only. On Day 1, changing the albedo, roughness length, and soil moisture content in the forested area has a pronounced effect on cloud development in

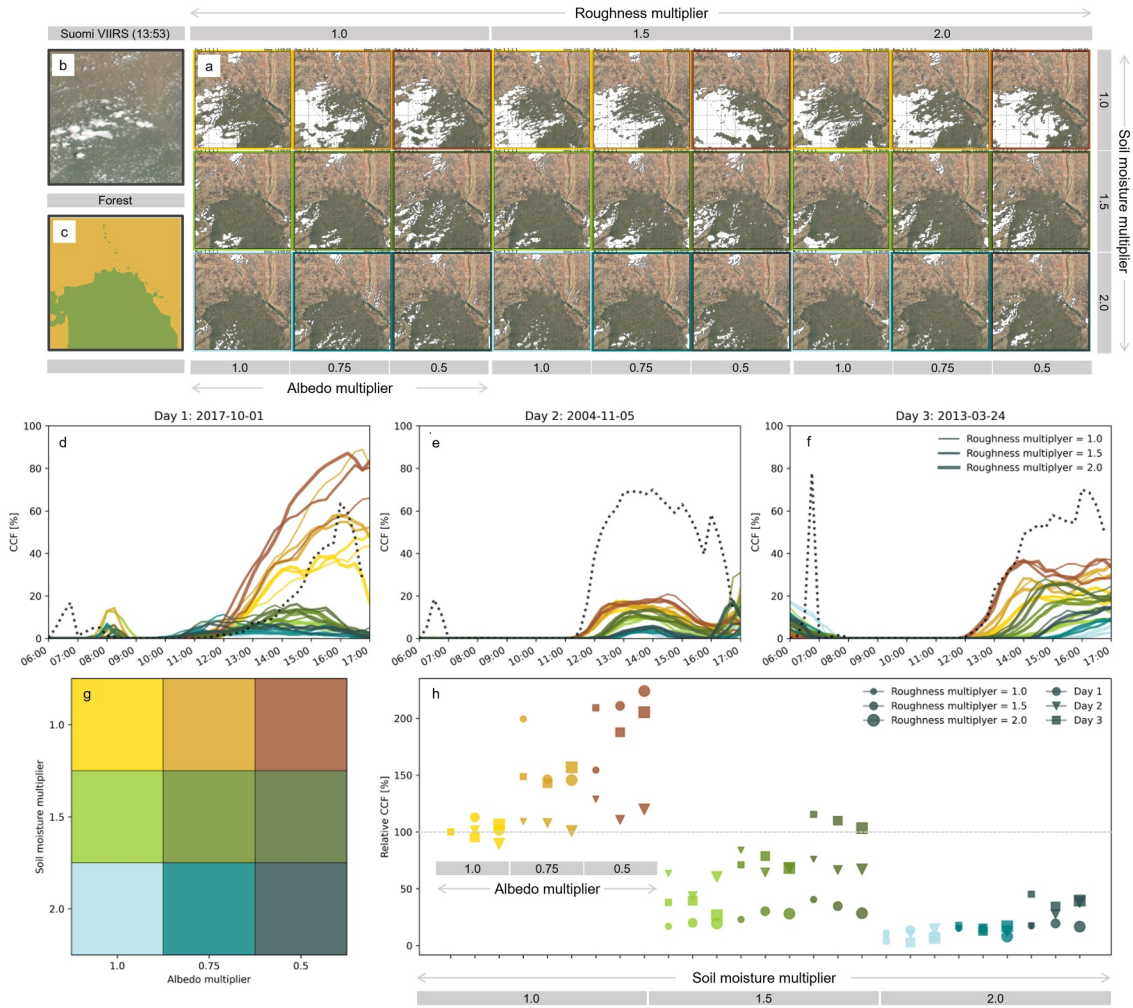

Figure 3. (a) Cloud cover (white) under different parameter combinations on Day 1 (1 October 2017) at 14:00 UTC in Domain 4. The parameter combination is indicated at the top (roughness multiplier), side (soil moisture multiplier), and bottom (albedo multiplier). The background image is obtained from Google Earth (Map data: Google, NASA). (b) As a reference, the image on the left shows Suomi VIIRS reflectance image at 1 October 2017 13:53 UTC in Domain 4 (Wolfe et al., 2013). The parameters are only changed in the forested areas indicated in (c). (d–f) Cloud cover fraction (CFF) over the course of the day for Day 1, Day 2, and Day 3 over the forested area. Line colors indicate different parameter combinations of albedo and soil moisture as shown in (g), while the line thickness indicates different surface roughness parameter multipliers. The black dotted line indicates the observed CCF, based on Ruijsch, Taylor, et al. (2025). (h) The afternoon (12:00–17:00 UTC) average CCF for the combinations of the albedo, soil moisture and surface roughness multipliers. The CCF is shown compared to the reference scenario, which has a value of 100%.

the case study area. Visual inspection of the model simulations reveals an enhanced cloud formation over the forest compared to the grassland, which is also visible in observational data (Figures 3a–3c). Cloud cover is especially prevalent in the south-western part of the forest. For all parameter combinations, clouds start developing around 12:00 UTC, reaching a maximum cloud cover around 14:00–16:00 UTC (Figure 3d).

Compared to the reference simulation, a decrease in albedo or an increase in surface roughness increases cloud formation in the forested region. Multiplying the albedo in the forested region by 0.75 and 0.5 increases the afternoon (12:00–17:00 UTC) average cloud cover in the forested region with, respectively, +99.4% and +54.4% (Figure 3h) compared to the reference albedo. Increasing the surface roughness has a smaller effect on cloud formation, as multiplying the roughness length by 1.5 results in a decrease in cloud cover of −12.9%, whereas multiplying it by 2.0 increases the cloud cover by +1.9%. Increasing the soil moisture in the forested regions strongly inhibits cloud formation (Figures 3a and 3d). Compared to the reference simulation, multiplying the soil moisture content by 1.5 and 2.0 results in a strong cloud cover decrease of, respectively, −83.1% and −90.0%.

Comparing all parameter combinations, the afternoon cloud cover fraction varies between +123.9% and −92.1% compared to the reference simulation.

The other case study days show a similar effect of changing the albedo, roughness length and soil moisture on cloud formation (Figures S8 and S9 in Supporting Information S1). However, even though observational data shows a similar cloud cover as Day 1, both Day 2 and Day 3 show a lower cloud cover over the course of the day (Figures 3d–3f). Yet, similar to Day 1, decreasing the albedo and increasing the roughness length results in an increase in cloud formation, whereas increasing the soil moisture reduces cloud formation. Interestingly, during these case study days, the maximum cloud cover is reached later during the day when the soil moisture is increased (Figures 3d–3f). In general, decreasing the albedo and increasing the surface roughness thus enhances and advances cloud formation, whereas increasing the soil moisture strongly reduces and delays cloud formation. Yet, increasing surface roughness can also decrease cloud formation in some cases.

3.3. Potential Underlying Mechanisms for Cloud Formation

To determine potential underlying mechanisms for cloud formation over the forested region, we determined how changing the albedo, roughness length, and soil moisture affects the surface energy balance, boundary layer development and mesoscale circulation. To determine why cloud formation is more pronounced over the forested region, we focus on the difference between the forest and grassland areas (Figure 4). A lower albedo in the forest region results in an increase in sensible heat flux and, to a lesser extent, in latent heat flux for all case study days (Figures 4a–4f). The latent heat flux is higher over the forested region over the course of the day, whereas the sensible heat flux is higher over the forested region until around 13:00 on Day 1, after which the sensible heat flux is higher over the grassland. During the other case study days, both the sensible and latent heat fluxes are higher over the forest region. A similar pattern can be seen in the boundary layer height (Figures 4g–4i). At the same time, the LCL is lower over the forest than over the grassland (Figures 4j–4o). In addition, the decreased albedo results in a higher vertical velocity over the forested area (Figures 4p–4r), which, combined with the higher boundary layer and lower LCL, results in a higher cloud formation in the forest compared grassland (Figures 4s–4).

Increasing the soil moisture in the forested region has a strong impact on surface energy balance and boundary layer development (Figure 4). A higher soil moisture results in an increased latent heat flux and decreased sensible heat flux in the forest compared to the grassland (Figures 4a–4f). The difference in boundary layer height between the forest and grassland is lower, or even negative (Figures 4g–4i), while the LCL decreases in both forest and grassland (Figures 4j–4l). As a result, the difference between the boundary layer height and LCL decreases on Day 1 and Day 2, and shows a delayed effect on Day 3 (Figure 4m–4o, Figures S10m–S10o and S11m–S11o in Supporting Information S1). A decrease in vertical velocity over the forest area can be observed, where the forest afternoon average turns from positive (rising air) for the dry soil to negative (sinking air) with the wet soil during Day 1 and 2 (Figures 4p–4r, Figures S10p–S10r in Supporting Information S1). Interestingly, increasing the soil moisture content not only decreases the cloud development over the forested area, but it becomes stronger over the grassland area than over the forest (Figures 4s–4u). Changing the surface roughness has a limited impact with variable sign on the sensible and latent heat flux and boundary layer development during all three case study days. However, the model simulations show generally stronger vertical wind velocities under simulations with a higher surface roughness (Figures 4p–4r). The ability of surface roughness to increase both the sensible and latent heat flux makes it difficult to predict the exact processes leading to increasing or decreasing cloud formation under surface roughness variations.

On Day 2 and Day 3, the cloud formation results in limited precipitation throughout the day, with a maximum cumulative precipitation of 0.16 mm. On Day 1, however, changing the albedo, surface roughness and soil moisture results in precipitation changes with similar patterns as the cloud cover (Figures 4v–4x). The maximum cumulative precipitation in the forested area (4.83 mm) is found with a maximum surface roughness, minimum albedo and minimum soil moisture. Whereas an increase in soil moisture strongly reduces the cumulative precipitation to 0.003 mm. Increasing the soil moisture does, however, increase the precipitation in the grassland regions to 1.15 mm (Figures S10 and S11 in Supporting Information S1).

To provide more insight into the difference in cloud formation mechanisms between a dry soil (reference soil moisture) and wet soil (soil moisture multiplied by 2.0 in the forest domain), we created a transect from the south-west (11.8°N, 1.8°E) to north-east (13.0°N, 3.0°E) within the model domain, roughly aligned with the wind direction (Figure 5). Just before the onset of cloud development, the south-western grassland part of the transect

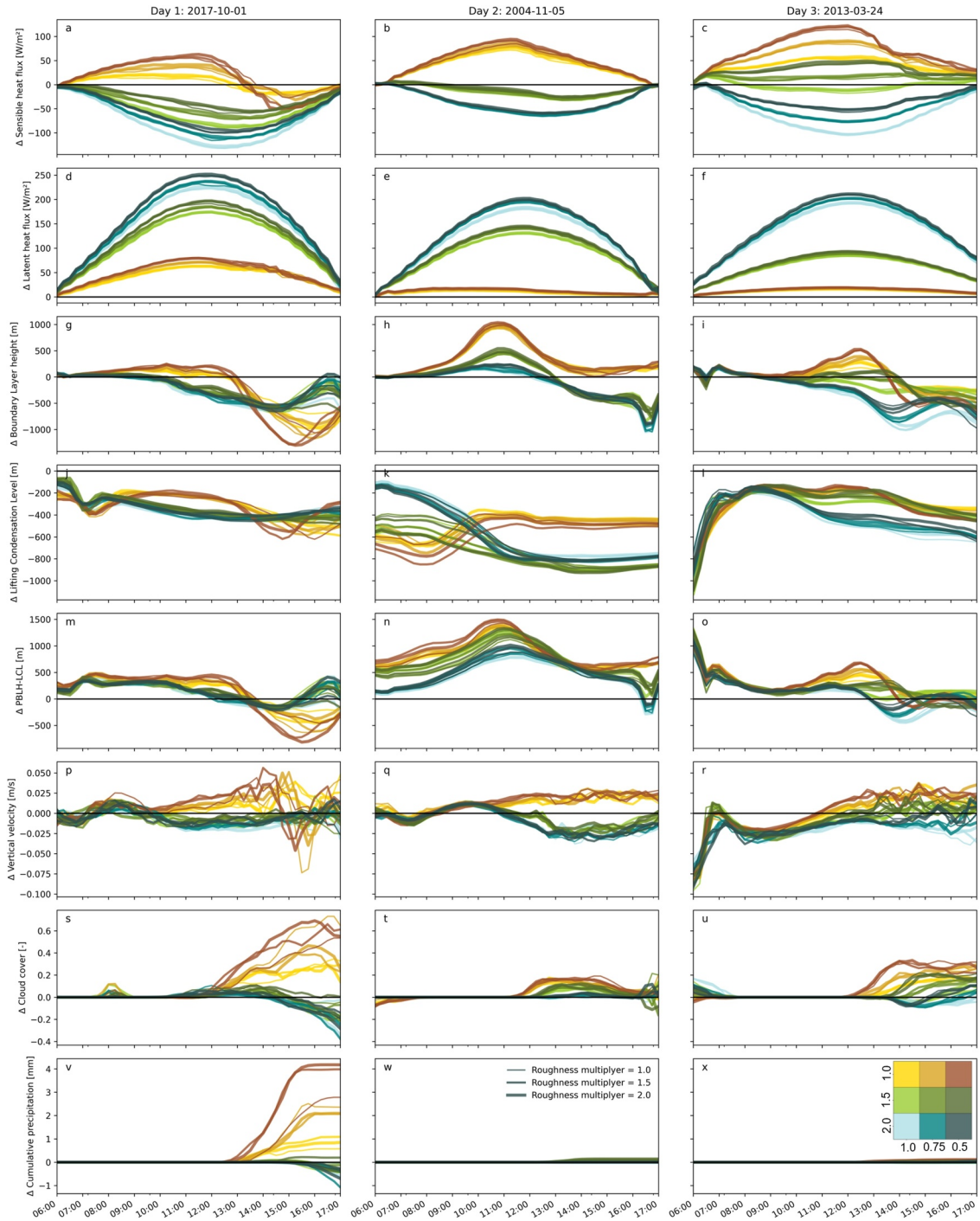

Figure 4. Effect of surface properties on surface fluxes, boundary layer growth and precipitation. Difference in (a–c) surface sensible heat flux, (d–f) surface latent heat flux, (g–i) boundary layer height, (j–l) lifting condensation level (LCL), (m–o) difference between boundary layer height and LCL, (p–r) vertical velocity, (s–u) cloud cover fraction and (v–x) cumulative precipitation between the forest and grassland area over the course of Day 1, Day 2, and Day 3 (06:00–17:00 UTC). The colors are similar to Figure 3. The inset in (x) shows the color legend with albedo (horizontal) and soil moisture (vertical) multipliers. Positive values indicate the value is higher in the forest area.

(left) has a relatively cool and moist atmosphere, whereas the north-eastern grassland part of the transect has a dryer and warmer atmosphere. When the soil moisture is low, the atmosphere over the forested region is relatively warm and dry, whereas under high soil moisture, the potential temperature gradually increases from the south-

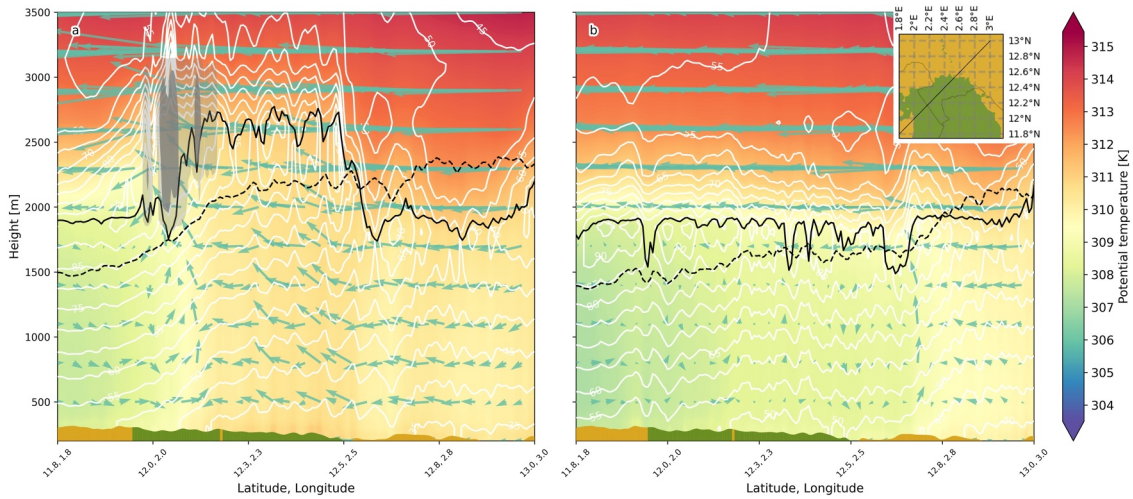

Figure 5. Vertical cross section of boundary layer development over dry and wet soils. The vertical velocity (blue arrows), relative humidity (white lines), and potential temperature (color) across height above sea level over a transect across the study domain on Day 1 at 12:45 UTC under (a) dry soil and (b) wet soil conditions. The colors on the bottom show topography and forest (green) and grassland (yellow). The planetary boundary layer height is indicated with the continuous black line, and the lifting condensation level with the dotted black line. The dry soil conditions are represented by the run with maximum albedo, minimum soil moisture, and maximum surface roughness. The wet soil conditions have a maximum albedo, maximum soil moisture, and maximum surface roughness.

west to the north-eastern part of the transect, consistent with the large-scale meridional temperature gradient that characterizes the Sahel.

Under dry soil conditions, the LCL increases from 1,469 m to a maximum of 2,386 m over the forest and north-western grassland region in the south-west of the domain. The boundary layer reaches as high as 2,774 m, compared to a maximum of 2,199 m over the grassland. Under wet soil conditions, the boundary layer has a relatively constant height with an average height of 1,850 m, while the LCL gradually increases from 1,370 to 2,145 m in the north-eastern grassland. In addition, under dry soil conditions, the wind speed near the surface is higher, with strong vertical velocities and wind convergence near the forest-grassland edge in the south-western part of the domain, which is not present under wet soil conditions.

3.4. Effect of Land Restoration Patterns on Cloud Formation

As a first step in determining the impact of land restoration pattern, the cloud formation over two baseline scenarios (100% grassland and 100% forest cover) was quantified. The grassland only scenario (0% forest cover) results in a low afternoon average cloud cover (3.2%), whereas the forest only scenario increases cloud cover to 8.4%. This suggests that forest itself increases cloud formation in this case study. Yet, when simulating cloud formation over 27 restoration scenarios with varying degrees of forest cover and clustering, the afternoon average cloud cover fraction varies between 4% (scenario in Figure 6a) and 25% (scenario Figure 6w), indicating that cloud formation is stronger over a combination of forest and grassland compared to only forest.

Visual inspection of the 27 restoration scenarios at 14:00 UTC shows that, for this case study, clouds are visibly more present under restoration scenarios with a higher spatial clustering (Figures 6j–6r) than with a more small-scale heterogeneous distribution of forest across the landscape (Figures 6a–6i). This is also shown by the afternoon average cloud cover fraction (Figure 6f1–6i1), although the exact combination of forest cover and clustering with the highest afternoon cloud cover is different per random variation (Figure S12 in Supporting Information S1). Under the highest clustering (Figures 6s–6a1), clouds develop especially at the edge between forest and grasslands (Movie S1).

Interestingly, increasing the amount of forest cover does not necessarily increase cloud formation in these scenarios. We find the highest cloud cover under scenarios with a high spatial clustering (more negative dispersion) and intermediate forest cover of 42.7% (e.g., Figure 6w), with an average afternoon cloud cover of 21.1% across the domain (Figure 6h1). Doubling the forest cover to 85.4%, strongly reduces the cloud cover to 14.4%. The highest cloud cover fraction appears where the forest patches have a length scale of 64 km (i.e., the average length

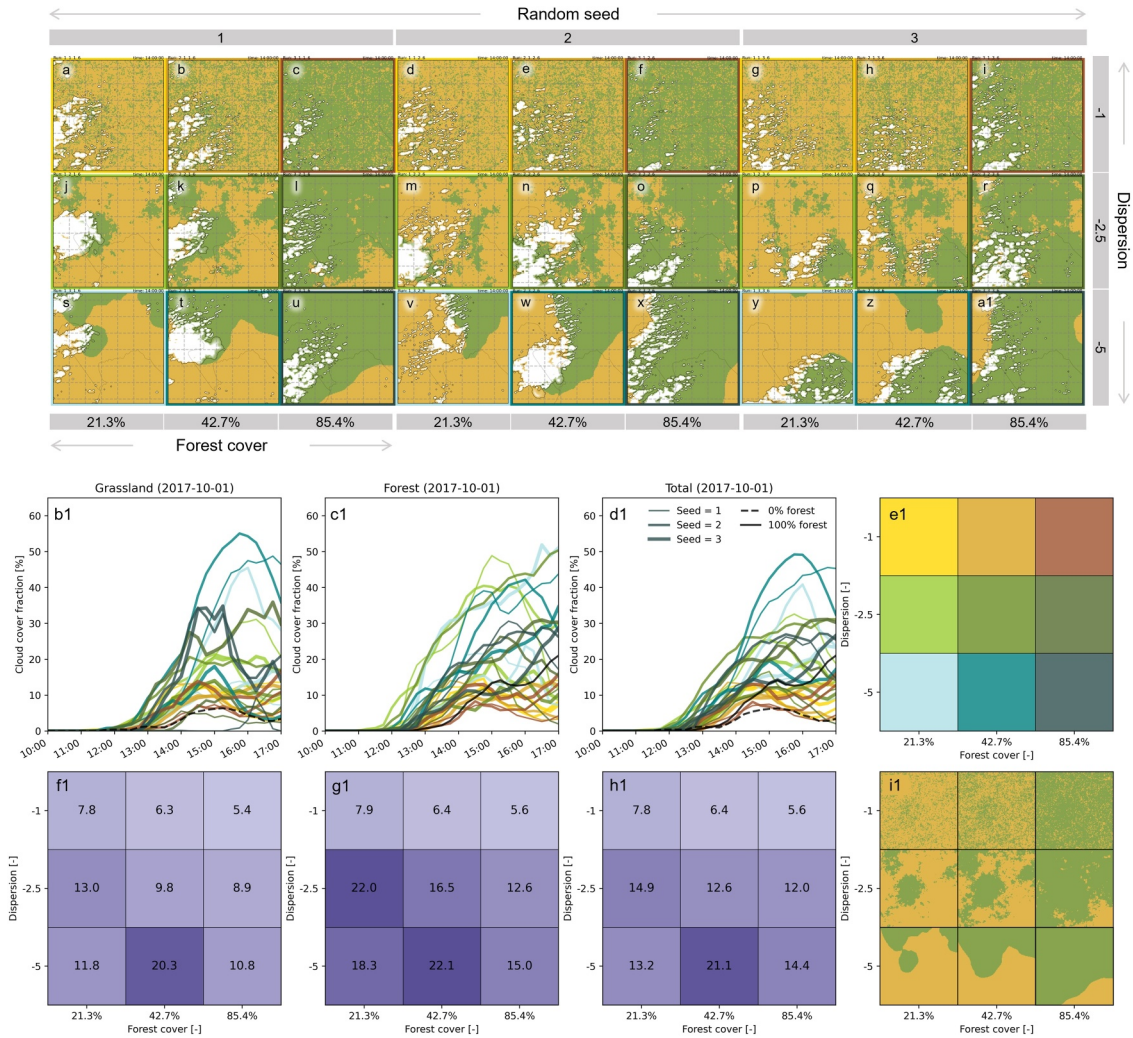

Figure 6. Effect of restoration design on cloud development. Cloud cover (white) under different restoration scenarios on Day 1 (1 October 2017) at 14:00 UTC in Domain 4. The background image shows the created land cover map, with forest in green and grassland in yellow, with different forest cover (indicated at the bottom), spatial dispersion (indicated on the right, more negative values indicate higher clustering) and random variations (indicated at the top), resulting in 27 land cover simulations. Movie S1 shows the cloud development between 09:00 and 15:00 UTC. Cloud cover fraction over the course of the day (b1) over the grassland, (c1) over the forest, and (d1) over the total domain. The line colors indicate different restoration scenarios with varying forest cover and spatial dispersion, as shown in (e1). Afternoon (12:00–17:00 UTC) average cloud cover fraction (%) (f1) over the grassland, (g1) over the forest, and (h1) over the total domains for the same restoration scenarios. The values show the average across the random seeds. Values for the separate seeds are visualized in Figure S12 in Supporting Information S1. The black striped and continuous line represents the 0% and 100% forest cover scenarios, respectively.

of forest across 1,000 random transects across the domain). This suggests that, although forests itself increase cloud formation in this case study, land cover variation with a longer length scale (i.e., clustered forest) can enhance cloud formation beyond a 100% forest cover.

To provide insight into the underlying mechanism for cloud enhancement over clustered forest patches, several surface and boundary layer variables were studied. This shows that the spatial pattern of forest has little influence on the area-averaged sensible and latent heat flux when the forest and grassland regions are considered separately (Figures 7a, 7b, 7e, and 7f). In contrast, total forest cover does impact the model domain-average fluxes, with higher sensible heat flux and lower latent heat flux as forest cover increases (Figures 7c and 7g). Because net radiation differs only slightly between forest and grassland until 12:00 UTC, these changes are primarily driven by differences in how the net radiation is partitioned between the turbulent fluxes (Figure S13 in Supporting Information S1). Up to the onset of cloud formation (around 12:00 UTC), also the boundary layer height and LCL develop similarly across the different land cover scenarios, and the boundary layer reaches the LCL around 12:00

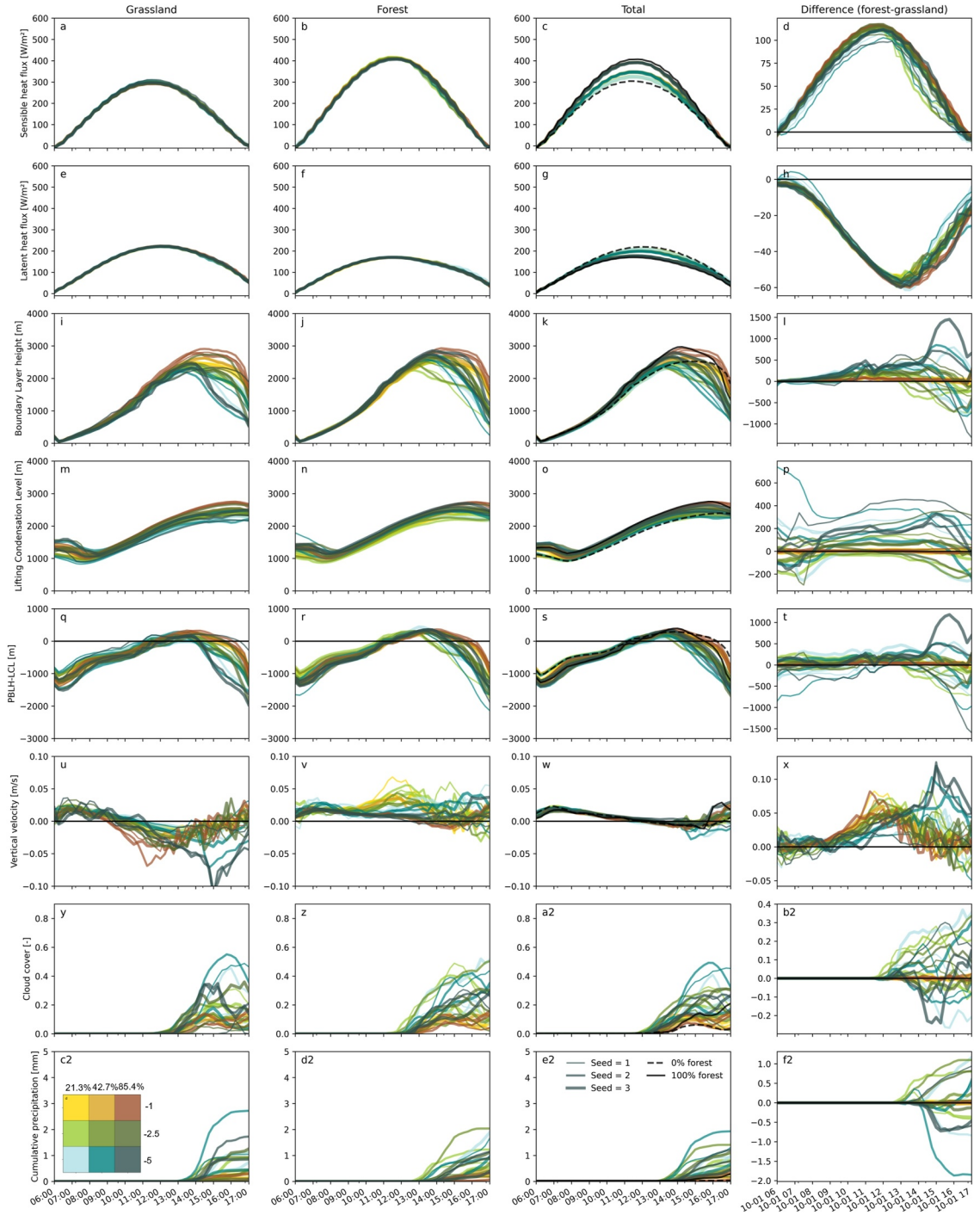

Figure 7. Diurnal variation in the grassland, the forest, the total domain and the difference between the forest and grassland for (a–d) sensible heat flux, (e–h) latent heat flux, (i–l) boundary layer height, (m–p) lifting condensation level (LCL), (q–t) difference between boundary layer height and LCL, (u–x) vertical wind velocity, (y–b2) cloud cover fraction and (c2–f2) cumulative precipitation between the forest and grassland area over the course of Day 1, Day 2, and Day 3 (06:00–17:00 UTC). Positive values indicate the value is higher in the forest area. The black striped and continuous line represents the 0% and 100% forest cover scenarios, respectively. The colors are similar to Figure 6. The inset in (c2) shows the color legend with forest cover (horizontal) and dispersion (vertical) values.

UTC (Figures 7i–7t). After 13:00 UTC, the boundary layer continues to grow for the small-scale heterogeneous forest cover, while the average boundary layer height strongly decreases under clustered forests, possibly as a result a smaller downwelling shortwave radiation due to the cloud formation itself (Figure S13 in Supporting Information S1). At the same time, land restoration configurations with the highest cloud cover show a more

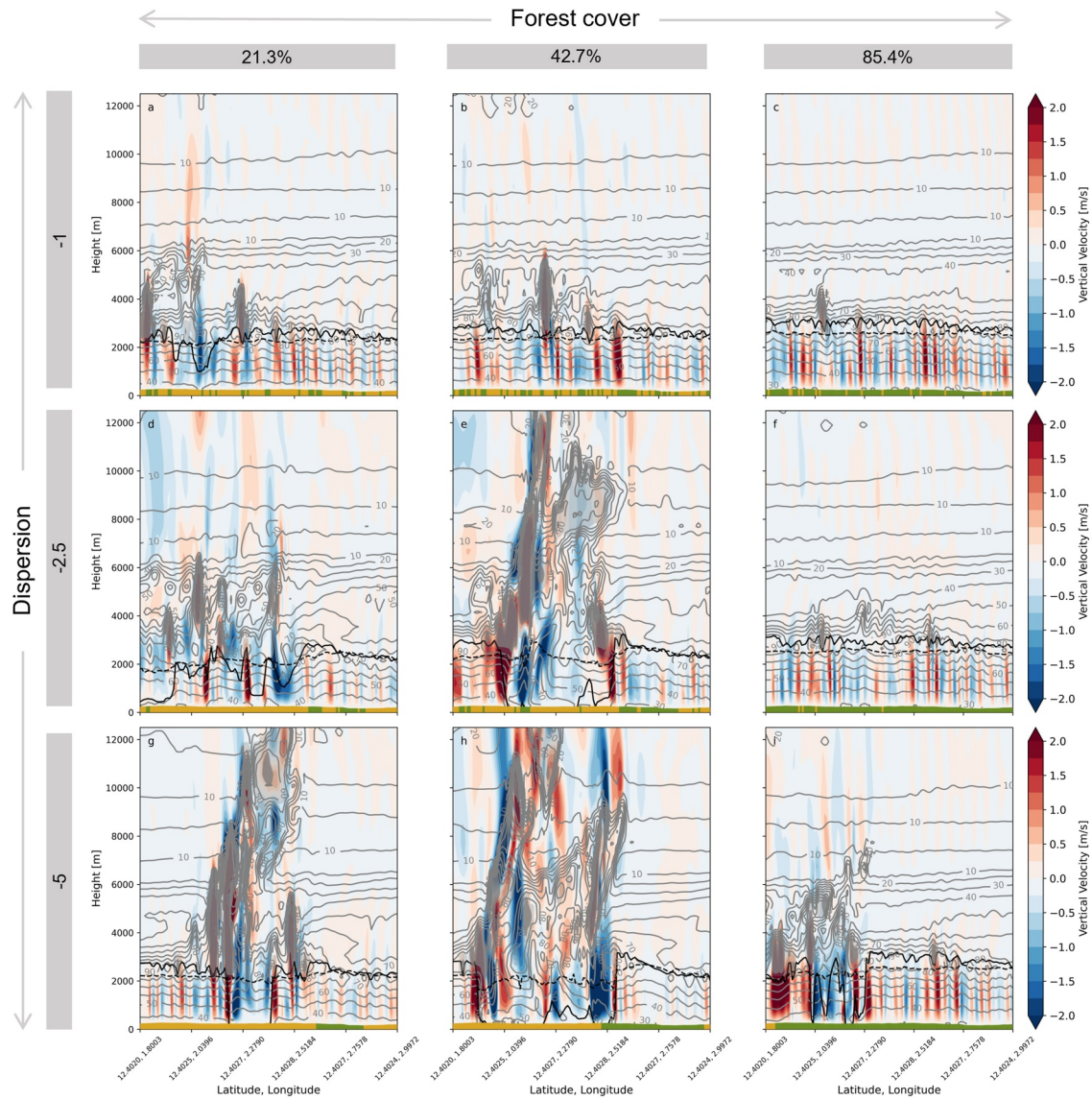

Figure 8. Vertical cross-section of boundary layer development over different spatial patterns of restoration. Vertical wind velocity (colors) at a west (left)-east (right) vertical cross section at a latitude of 12.4°N at 14:15 UTC for nine different restoration scenarios corresponding to Random Seed 2 in Figure 6. The black continuous line indicates the boundary layer height, the striped black line the lifting condensation lever and the gray lines the relative humidity contours (%). The land cover type is indicated by the yellow (grass) and green (forest) shading at the bottom. The gray opaque and transparent shading indicates a cloud water mixing ratio of, respectively, more than 0.001 and 0.1 g/kg. The blue shading indicates a precipitation mixing ratio of the same values.

negative (downward) vertical velocity over the grassland and a positive (upward) vertical velocity over the forest, especially at the end of the afternoon (Figures 7u–7b2).

Because the boundary layer development is similar across restoration scenarios, we study a vertical transect across the model domain for nine of the different spatial configurations with varying forest cover and spatial clustering, which provides more insight into the impact of mesoscale circulations (Figure 8). The nine transects correspond to Random Seed 2 in Figure 6.

At 14:15 UTC, relatively shallow clouds have developed over a small-scale heterogeneous forest cover (Figures 8a–8c) and the high forest cover scenarios (Figures 8c, 8f, and 8i). At the edges of larger forest patches, high equivalent potential temperatures (Figure S14 in Supporting Information S1), near-surface wind convergence and a strong reduction in boundary layer height have developed, with a strong upward vertical velocity at the cloud edges, and a downward wind at the center, corresponding to the decrease in boundary layer height over

clustered observed in Figures 7i–7l. Over the clustered forest, especially with intermediate and lower forest cover, we find the development of deep convection, with clouds reaching as high as 12 km (Figures 8e, 8g, and 8h). These clouds first develop at the forest-grassland edge and later expand mainly into the grassland (Movie S2).

The cloud formation in this case study also results in precipitation, with, in general, a higher cumulative precipitation for configurations with a high cloud cover and more spatial clustering (Figures 7y–7f2). Inside the forest, we find the highest average cumulative precipitation under scenarios with a high spatial clustering and the lowest forest cover (seed 3), with 1.89 mm. A low spatial clustering generally results in an average cumulative precipitation between 0.43 and 0.05 mm. All these scenarios have, however, a higher cumulative precipitation than the scenario with only grass (0.03 mm).

4. Discussion and Conclusions

In this study, we used the WRF atmospheric model to determine how the spatial pattern of land restoration projects impacts cloud formation in West African drylands. We selected three case study days that show an enhanced cloud formation over the W-Arly-Pendjari Complex at the border of Benin, Niger and Burkina Faso, and ran the model with varying albedo, surface roughness and soil moisture content to determine mechanisms behind observed cloud formation over forested regions and how these parameters impact cloud formation. According to existing research, clouds can either be enhanced or inhibited over forested regions. In temperate regions, observational analysis has shown cloud enhancement over forest, while in some parts of the Amazon, the high evapotranspiration of forests inhibits cloud formation (Duveiller et al., 2021; Xu et al., 2022). The low albedo and high surface roughness over forests increase boundary layer growth, which can result in enhanced cloud formation over regions with a high sensible heat flux (Bosman et al., 2019; Teuling et al., 2017). In addition, the high evaporation provides atmospheric moisture and lowers the LCL, enhancing cloud formation over regions with a high evaporation if the sensible heat flux is large enough to stimulate boundary layer growth (Findell & Eltahir, 2003; Garcia-Carreras et al., 2017).

In this study, model simulations show that increasing the surface roughness and albedo inside the forest enhances the afternoon cloud cover fraction up to +123.9% due to the increased net radiation and sensible heat flux. During these simulations, the sensible heat flux and boundary layer height are larger over the forested region than over the surrounding grassland. Similar results have been found for case studies in Europe, where the high sensible heat flux is essential to for the onset of cloud development over forested regions (Bosman et al., 2019; Noual et al., 2023). However, increasing the soil moisture content in the forest strongly reduces the cloud formation, up to −97.2%, over the forest. Because the evapotranspiration in dryland regions is strongly water-limited, increasing the soil moisture content strongly enhances the latent heat flux in the forest region, at the expense of the sensible heat flux, resulting in a lower boundary layer compared to the grassland region. Thus, under dry soil moisture conditions, the forest has a higher sensible heat flux, boundary layer growth and cloud formation. Under wet soil moisture conditions, the forest region has a lower sensible heat flux, boundary layer and cloud formation than the surrounding grassland region, which is in line with the negative relationships between soil moisture and cloud formation in West Africa as found in other studies (Klein & Taylor, 2020; Taylor et al., 2012, 2013). Based on these results, an increase in sensible heat flux appears to be more critical for cloud formation than a decrease in atmospheric moisture, again in line with Bosman et al. (2019) and Noual et al. (2023).

In addition, differences in surface roughness and albedo between the forest and adjacent grassland can trigger thermally and dynamically driven mesoscale circulations, which enhance cloud formation over warm and rough regions (Birch et al., 2014; Khanna & Medvigy, 2014; Spracklen et al., 2018). In this study, the relatively high soil moisture in the south-western part of the case study domain (Figure S1 in Supporting Information S1) in combination with the dry and dark forest, cause a sharp contrast in boundary layer height and potential temperature, resulting in updraft and wind convergence, and ultimately cloud formation, at the forest-grassland edge. During the wet soil conditions, wind convergence and mesoscale circulation needed for cloud development do not develop in the same way as during dry soil conditions. This suggests that these circulations play an important role in cloud development, at least during the case study days. Although these only represent conditions during these three case study days, observations show enhanced cloud formation over regions with a negative soil moisture anomaly due to the enhanced sensible heat flux over longer time scales (Taylor et al., 2011, 2012).

To determine the effect of spatial patterns of restoration, we ran 27 land restoration scenarios with varying forest cover and spatial clustering. Model simulations show that a more clustered forest cover results in cloud cover

enhancement compared to a more small-scale heterogeneous forest. Furthermore, clustered patches of forests (alternated with grassland) increase cloud development compared to a completely forested domain. This suggests that a certain degree of variation in land cover, of certain length scales, increases cloud formation in this region. Since the latent and sensible heat fluxes are similar over both clustered and small-scale heterogeneous forest cover, the differences in cloud formation are likely driven by other mechanisms, such as mesoscale circulation and convergence at the boundaries of the clustered forests. The variation in surface roughness and temperature of the boundary layer over the forest and grassland contributes to thermally (temperature) and dynamically (roughness) driven mesoscale circulations caused by frictional convergence, resulting in cloud formation on the forest-grassland boundary. In addition, these heterogeneities provide favorable conditions for convection and rainfall (Garcia-Carreras & Parker, 2011). Similar results were seen with observational data, where only larger protected areas in West Africa show cloud enhancement (Ruijsch, Taylor, et al., 2025). Other observational and modeling studies have shown mesoscale circulation to cause cloud cover enhancement over the warm and rough edge of land cover heterogeneities (Ascher et al., 2025; Garcia-Carreras et al., 2010; Spracklen et al., 2018; Taylor et al., 2022a), which is, in this case, the forested side due to the relatively dry soil.

As the sensitivity analysis highlights that cloud formation is strongly coupled to soil moisture heterogeneities, it is, however, expected that the cloud enhancement under the different land restoration scenarios varies with soil moisture conditions and throughout the year. Other studies have indeed found that the effect of deforestation strongly depends on seasonality in Asia and South America (Leung et al., 2024; Qin et al., 2025). In addition, multi-year satellite observations show that the relative difference in cloud cover fraction between the forest and grassland in a similar case study region is 8%, which is lower than the strong cloud enhancement during these specific case study days. While computational limitations restricted longer model simulations, further research on the overall long-term effect of the patterns of land restoration on cloud formation would therefore be insightful. This will also provide more insights into potential feedbacks, both between soil moisture and cloud formation, and to the vegetation itself. In addition, because this is a modeling study, the accuracy of the representation of the model and the input data results also impacts the accuracy of the results. Comparisons with radiosonde and satellite data indicate a systematic underestimation of cloud cover fraction, likely related to an overly dry boundary layer and soil moisture, which may have resulted in a underestimation of evaporation and too high LCL. Yet, as limited flux measurements are available in the study region, in-depth validation of the surface energy balance is challenging. On top of that, higher resolution model simulations using, for example, Large Eddy Simulation may provide more accurate patterns of cloud cover because these models are able to mostly resolve turbulent structures and shallow cumulus clouds in the atmospheric boundary layer (Honnert et al., 2020). Despite the underestimation of cloud cover fraction, especially on Day 2 and 3, this study provides insight into what extent soil moisture, surface roughness and albedo impact cloud enhancement over vegetated regions.

This study shows that spatial patterns of land restoration projects strongly influence cloud formation, with a stronger cloud enhancement of vegetation over clustered forests. This suggests that, if cloud (or rainfall) enhancement is a goal of the project, larger patches of forest (e.g., protected areas) in a grassland region are more effective in generating clouds than smaller patches of forests (e.g., farmer-managed natural regeneration). Although the small-scale heterogeneous forest cover does not result in a considerable increase in cloud cover compared to grassland only, the results do show an increased cumulative precipitation with small-scale heterogeneous forest cover (up to 0.43 mm) compared to the grassland simulation (0.03 mm). A high spatial clustering can, however, increase the domain-averaged cumulative precipitation up to 1.89 mm. This study, therefore, suggests that restoration can locally impact water availability, as found in previous global analyses (e.g., Hoek van Dijke et al., 2022). It should be noted, however, that this study only considers two land cover classes (forest and grassland) to limit the number of variables. A landscape with a higher species diversity may, however, be more suitable for restoration practices, especially in dryland ecosystems where large forest patches are not native (Bond et al., 2019; Parr et al., 2024; Veldman et al., 2015). Future research could therefore focus how more realistic and diverse model scenarios affect the results in this study.

Nonetheless, this research can provide insights for policymakers on how the design of restoration projects in West African drylands impacts cloud cover or precipitation. In addition, given the many restoration projects currently being implemented under, for example, the United Nations Decade of Ecosystem Restoration or the Great Green Wall of Africa, and the strong effect of changes in cloud cover on the global climate (Goessling et al., 2025), both through trapping heat emitted by the Earth's surface and reflecting incoming solar radiation, more insight into the

cloud impacts of land restoration projects is essential to understand their overall climate effect and look beyond their carbon sequestration potential (Ibisch et al., 2025).

Conflict of Interest

The authors declare no conflicts of interest relevant to this study.

Data Availability Statement

The WRF model is available at https://github.com/wrf-model/WRF.git. Radiosonde data is obtained from https://weather.uwyo.edu/upperair/sounding_legacy.html. The WRF namelist.input and namelist.wps files and the scripts to run the sensitivity analysis and restoration scenarios with the WRF model area available at https://doi.org/10.6084/m9.figshare.29136776 (Ruijsch, Teuling, et al., 2025). Also the used validation data and average cloud cover fraction are available in this data set.

Acknowledgments
The authors also thank the anonymous reviewers for there useful comments. This research is funded by the SUBACA foundation.

References

Achugbu, I. C., Dudhia, J., Olufayo, A. A., Balogun, I. A., Adefisan, E. A., & Gbode, I. E. (2020). Assessment of WRF land surface model performance over West Africa. *Advances in Meteorology*, *2020*(1), 6205308. https://doi.org/10.1155/2020/6205308

Ascher, B. D., Saleeby, S. M., Marinescu, P. J., & van den Heever, S. C. (2025). Forest breeze–cold pool interactions drive convective organization over heterogeneous vegetation. *Journal of the Atmospheric Sciences*, *82*(1), 71–94. https://doi.org/10.1175/JAS-D-24-0084.1

Birch, C. E., Marsham, J. H., Parker, D. J., & Taylor, C. M. (2014). The scale dependence and structure of convergence fields preceding the initiation of deep convection. *Geophysical Research Letters*, *41*(13), 4769–4776. https://doi.org/10.1002/2014GL060493

Bonan, G. B. (2008). Forests and climate change: Forcings, feedbacks, and the climate benefits of forests. *Science*, *320*(5882), 1444–1449. https://doi.org/10.1126/science.1155121

Bond, W. J., Stevens, N., Midgley, G. F., & Lehmann, C. E. R. (2019). The trouble with trees: Afforestation plans for Africa. *Trends in Ecology & Evolution*, *34*(11), 963–965. https://doi.org/10.1016/j.tree.2019.08.003

Bosman, P. J., van Heerwaarden, C. C., & Teuling, A. J. (2019). Sensible heating as a potential mechanism for enhanced cloud formation over temperate forest. *Quarterly Journal of the Royal Meteorological Society*, *145*(719), 450–468. https://doi.org/10.1002/qj.3441

Broxton, P. D., Zeng, X., Sulla-Menashe, D., & Troch, P. A. (2014). A global land cover climatology using MODIS data. *Journal of Applied Meteorology and Climatology*, *53*(6), 1593–1605. https://doi.org/10.1175/JAMC-D-13-0270.1

Chen, F., & Avissar, R. (1994). Impact of land-surface moisture variability on local shallow convective cumulus and precipitation in large-scale models. *Journal of Applied Meteorology and Climatology*, *33*(12), 1382–1401. https://doi.org/10.1175/1520-0450(1994)033<1382:IOLSMV>2.0.CO;2

Chen, S., Haase, D., Qureshi, S., & Firozjaei, M. K. (2022). Integrated land use and urban function impacts on land surface temperature: Implications on urban heat mitigation in Berlin with eight-type spaces. *Sustainable Cities and Society*, *83*, 103944. https://doi.org/10.1016/j.scs.2022.103944

Cook-Patton, S. C., Leavitt, S. M., Gibbs, D., Harris, N. L., Lister, K., Anderson-Teixeira, K. J., et al. (2020). Mapping carbon accumulation potential from global natural forest regrowth. *Nature*, *585*(7826), 545–550. https://doi.org/10.1038/s41586-020-2686-x

Duveiller, G., Filipponi, F., Ceglar, A., Bojanowski, J., Alkama, R., & Cescatti, A. (2021). Revealing the widespread potential of forests to increase low level cloud cover. *Nature Communications*, *12*(1), 4337. https://doi.org/10.1038/s41467-021-24551-5

Duveiller, G., Hooker, J., & Cescatti, A. (2018). The mark of vegetation change on Earth's surface energy balance. *Nature Communications*, *9*(1), 679. https://doi.org/10.1038/s41467-017-02810-8

Ek, M. B., & Holtslag, A. A. M. (2004). Influence of soil moisture on boundary layer cloud development. *Journal of Hydrometeorology*, *5*(1), 86–99. https://doi.org/10.1175/1525-7541(2004)005<0086:IOSMOB>2.0.CO;2

Feldman, A. F., Short Gianotti, D. J., Dong, J., Trigo, I. F., Salvucci, G. D., & Entekhabi, D. (2022). Tropical surface temperature response to vegetation cover changes and the role of drylands. *Global Change Biology*, *29*(1), 110–125. https://doi.org/10.1111/gcb.16455

Findell, K. L., & Eltahir, E. A. (2003). Atmospheric controls on soil moisture–boundary layer interactions. Part I: Framework development. *Journal of Hydrometeorology*, *4*(3), 552–569. https://doi.org/10.1175/1525-7541(2003)004

Garcia-Carreras, L., Marsham, J. H., & Spracklen, D. V. (2017). Observations of increased cloud cover over irrigated agriculture in an arid environment. *Journal of Hydrometeorology*, *18*(8), 2161–2172. https://doi.org/10.1175/Jhm-D-16-0208.1

Garcia-Carreras, L., & Parker, D. (2011). How does local tropical deforestation affect rainfall? *Geophysical Research Letters*, *38*(19). https://doi.org/10.1029/2011gl049099

Garcia-Carreras, L., Parker, D. J., Taylor, C. M., Reeves, C. E., & Murphy, J. G. (2010). Impact of mesoscale vegetation heterogeneities on the dynamical and thermodynamic properties of the planetary boundary layer. *Journal of Geophysical Research*, *115*(D3). https://doi.org/10.1029/2009JD012811

Goessling, H. F., Rackow, T., & Jung, T. (2025). Recent global temperature surge intensified by record-low planetary albedo. *Science*, *387*(6729), 68–73. https://doi.org/10.1126/science.adq7280

Grell, G. A., Dudhia, J., & Stauffer, D. R. (1994). *A description of the fifth-generation Penn State/NCAR Mesoscale Model (MM5)*. University Corporation for Atmospheric Research. https://doi.org/10.5065/D60Z716B

Hasler, N., Williams, C. A., Denney, V. C., Ellis, P. W., Shrestha, S., Terasaki Hart, D. E., et al. (2024). Accounting for albedo change to identify climate-positive tree cover restoration. *Nature Communications*, *15*(1), 2275. https://doi.org/10.1038/s41467-024-46577-1

Hoek van Dijke, A. J., Herold, M., Mallick, K., Benedict, I., Machwitz, M., Schlerf, M., et al. (2022). Shifts in regional water availability due to global tree restoration. *Nature Geoscience*, *15*(5), 363–368. https://doi.org/10.1038/s41561-022-00935-0

Holl, K. D., & Brancalion, P. H. (2020). Tree planting is not a simple solution. *Science*, *368*(6491), 580–581. https://doi.org/10.1126/science.aba8232

Hong, S.-Y., & Lim, J.-O. J. (2006). The WRF single-moment 6-class microphysics scheme (WSM6). *Asia-Pacific Journal of Atmospheric Sciences*, *42*(2), 129–151.

Hong, S.-Y., Noh, Y., & Dudhia, J. (2006). A new vertical diffusion package with an explicit treatment of entrainment processes. *Monthly Weather Review*, *134*(9), 2318–2341. https://doi.org/10.1175/mwr3199.1

Honnert, R., Efstathiou, G. A., Beare, R. J., Ito, J., Lock, A., Neggers, R., et al. (2020). The atmospheric boundary layer and the "Gray Zone" of turbulence: A critical review. *Journal of Geophysical Research: Atmospheres*, *125*(13), e2019JD030317. https://doi.org/10.1029/2019JD030317

Ibisch, P. L., Sheil, D., Baudena, M., Coumou, D., Dellasala, D., Ellison, D., et al. (2025). *Cloudy outlook for forests [eLetter]*. Science.

Jankov, I., Gallus, W. A., Segal, M., & Koch, S. E. (2007). Influence of initial conditions on the WRF–ARW model QPF response to physical parameterization changes. *Weather and Forecasting*, *22*(3), 501–519. https://doi.org/10.1175/WAF998.1

Khanna, J., & Medvigy, D. (2014). Strong control of surface roughness variations on the simulated dry season regional atmospheric response to contemporary deforestation in Rondônia, Brazil. *Journal of Geophysical Research: Atmospheres*, *119*(23), 13067–13078. https://doi.org/10.1002/2014JD022278

Kirschbaum, M. U. F., Cowie, A. L., Peñuelas, J., Smith, P., Conant, R. T., Sage, R. F., et al. (2024). Is tree planting an effective strategy for climate change mitigation? *Science of the Total Environment*, *909*, 168479. https://doi.org/10.1016/j.scitotenv.2023.168479

Kleczek, M. A., Steeneveld, G.-J., & Holtslag, A. A. M. (2014). Evaluation of the weather research and forecasting mesoscale model for GABLS3: Impact of boundary-layer schemes, boundary conditions and Spin-Up. *Boundary-Layer Meteorology*, *152*(2), 213–243. https://doi.org/10.1007/s10546-014-9925-3

Klein, C., Heinzeller, D., Bliefernicht, J., & Kunstmann, H. (2015). Variability of West African monsoon patterns generated by a WRF multi-physics ensemble. *Climate Dynamics*, *45*(9), 2733–2755. https://doi.org/10.1007/s00382-015-2505-5

Klein, C., & Taylor, C. M. (2020). Dry soils can intensify mesoscale convective systems. *Proceedings of the National Academy of Sciences of the United States of America*, *117*(35), 21132–21137. https://doi.org/10.1073/pnas.2007998117

Kristensen, J. Å., Barbero-Palacios, L., Barrio, I. C., Jacobsen, I. B. D., Kerby, J. T., López-Blanco, E., et al. (2024). Tree planting is no climate solution at northern high latitudes. *Nature Geoscience*, *17*(11), 1087–1092. https://doi.org/10.1038/s41561-024-01573-4

Lawrence, D., Coe, M., Walker, W., Verchot, L., & Vandecar, K. (2022). The unseen effects of deforestation: Biophysical effects on climate. *Frontiers in Forests and Global Change*, *5*, 756115. https://doi.org/10.3389/ffgc.2022.756115

Lennon, J. J. (2000). Red-shifts and red herrings in geographical ecology. *Ecography*, *23*(1), 101–113. https://doi.org/10.1111/j.1600-0587.2000.tb00265.x

Leung, G. R., Grant, L. D., & van den Heever, S. C. (2024). Deforestation-driven increases in shallow clouds are greatest in drier, low-aerosol regions of Southeast Asia. *Geophysical Research Letters*, *51*(10), e2023GL107678. https://doi.org/10.1029/2023GL107678

Lynn, B. H., Tao, W.-K., & Wetzel, P. J. (1998). A study of landscape-generated deep moist convection. *Monthly Weather Review*, *126*(4), 928–942. https://doi.org/10.1175/1520-0493(1998)126<0928:ASOLGD>2.0.CO;2

Martin, M. P., Woodbury, D. J., Doroski, D. A., Nagele, E., Storace, M., Cook-Patton, S. C., et al. (2021). People plant trees for utility more often than for biodiversity or carbon. *Biological Conservation*, *261*, 109224. https://doi.org/10.1016/j.biocon.2021.109224

Mathon, V., Laurent, H., & Lebel, T. (2002). Mesoscale convective system rainfall in the Sahel. *Journal of Applied Meteorology*, *41*(11), 1081–1092. https://doi.org/10.1175/1520-0450(2002)041

Miralles, D. G., van den Berg, M. J., Teuling, A. J., & de Jeu, R. A. M. (2012). Soil moisture-temperature coupling: A multiscale observational analysis. *Geophysical Research Letters*, *39*(21), L21707. https://doi.org/10.1029/2012GL053703

Noual, G., Brunet, Y., Le Moigne, P., & Lac, C. (2023). Simulating the effects of regional forest cover and windthrow-induced cover changes on mid-latitude boundary-layer clouds. *Journal of Geophysical Research: Atmospheres*, *128*(13), e2023JD038477. https://doi.org/10.1029/2023jd038477

Oreopoulos, L., & Barker, H. W. (1999). Accounting for subgrid-scale cloud variability in a multi-layer 1D solar radiative transfer algorithm. *Quarterly Journal of the Royal Meteorological Society*, *125*(553), 301–330. https://doi.org/10.1002/qj.49712555316

Parr, C. L., te Beest, M., & Stevens, N. (2024). Conflation of reforestation with restoration is widespread. *Science*, *383*(6684), 698–701. https://doi.org/10.1126/science.adj0899

PBL. (2020). Global restoration commitments database [Dataset]. Retrieved from https://www.pbl.nl/en/publications/goals-and-commitments-for-the-restoration-decade

Prăvălie, R. (2021). Exploring the multiple land degradation pathways across the planet. *Earth-Science Reviews*, *220*, 103689. https://doi.org/10.1016/j.earscirev.2021.103689

Qin, Y., Wang, D., Ziegler, A. D., Fu, B., & Zeng, Z. (2025). Impact of Amazonian deforestation on precipitation reverses between seasons. *Nature*, *639*(8053), 102–108. https://doi.org/10.1038/s41586-024-08570-y

Roe, S., Streck, C., Obersteiner, M., Frank, S., Griscom, B., Drouet, L., et al. (2019). Contribution of the land sector to a 1.5°C world. *Nature Climate Change*, *9*(11), 817–828. https://doi.org/10.1038/s41558-019-0591-9

Ruijsch, J., Taylor, C. M., Hutjes, R. W. A., & Teuling, A. J. (2025). Scale-dependent cloud enhancement from land restoration in West African drylands. *Communications Earth & Environment*, *6*(1), 174. https://doi.org/10.1038/s43247-025-02154-y

Ruijsch, J., Teuling, A. J., Duveiller, G., & Hutjes, R. W. A. (2024). The local cooling potential of land restoration in Africa. *Communications Earth & Environment*, *5*(1), 495. https://doi.org/10.1038/s43247-024-01650-x

Ruijsch, J., Teuling, A. J., Taylor, C. M., Steeneveld, G. J., & Hutjes, R. (2025). Clustered land restoration projects increase cloud formation in West African drylands [Dataset]. *figshare*. https://doi.org/10.6084/m9.figshare.29136776.v1

Skamarock, W. C., Klemp, J. B., Dudhia, J., Gill, D. O., Liu, Z., Berner, J., et al. (2019). *A description of the advanced research WRF model version 4* (p. 145) [*Report*]. National Center for Atmospheric Research.

Spracklen, D., Baker, J., Garcia-Carreras, L., & Marsham, J. (2018). The effects of tropical vegetation on rainfall. *Annual Review of Environment and Resources*, *43*(1), 193–218. https://doi.org/10.1146/annurev-environ-102017-030136

Taylor, C. M. (2015). Detecting soil moisture impacts on convective initiation in Europe. *Geophysical Research Letters*, *42*(11), 4631–4638. https://doi.org/10.1002/2015gl064030

Taylor, C. M., Birch, C. E., Parker, D. J., Dixon, N., Guichard, F., Nikulin, G., & Lister, G. M. S. (2013). Modeling soil moisture-precipitation feedback in the Sahel: Importance of spatial scale versus convective parameterization. *Geophysical Research Letters*, *40*(23), 6213–6218. https://doi.org/10.1002/2013GL058511

Taylor, C. M., de Jeu, R. A., Guichard, F., Harris, P. P., & Dorigo, W. A. (2012). Afternoon rain more likely over drier soils. *Nature*, *489*(7416), 423–426. https://doi.org/10.1038/nature11377

Taylor, C. M., Gounou, A., Guichard, F., Harris, P. P., Ellis, R. J., Couvreux, F., & De Kauwe, M. (2011). Frequency of Sahelian storm initiation enhanced over mesoscale soil-moisture patterns. *Nature Geoscience*, *4*(7), 430–433. https://doi.org/10.1038/ngeo1173

Taylor, C. M., Klein, C., Dione, C., Parker, D. J., Marsham, J., Abdoulahat Diop, C., et al. (2022). Nowcasting tracks of severe convective storms in West Africa from observations of land surface state. *Environmental Research Letters*, *17*(3), 034016. https://doi.org/10.1088/1748-9326/ac536d

Taylor, C. M., Klein, C., Parker, D. J., Gerard, F., Semeena, V. S., Barton, E. J., & Harris, B. L. (2022). "Late-stage" deforestation enhances storm trends in coastal West Africa. *Proceedings of the National Academy of Sciences*, *119*(2), e2109285119. https://doi.org/10.1073/pnas.2109285119

Taylor, C. M., Parker, D. J., & Harris, P. P. (2007). An observational case study of mesoscale atmospheric circulations induced by soil moisture. *Geophysical Research Letters*, *34*(15), 220. https://doi.org/10.1029/2007GL030572

Teuling, A. J., Taylor, C. M., Meirink, J. F., Melsen, L. A., Miralles, D. G., Van Heerwaarden, C. C., et al. (2017). Observational evidence for cloud cover enhancement over western European forests. *Nature Communications*, *8*(1), 14065. https://doi.org/10.1038/ncomms14065

Te Wierik, S. A., Keune, J., Miralles, D. G., Gupta, J., Artzy-Randrup, Y. A., Cammeraat, L. H., & van Loon, E. E. (2024). Critical importance of tree and non-tree vegetation for African precipitation. *Geophysical Research Letters*, *51*(20), e2023GL103274. https://doi.org/10.1029/2023GL103274

UNEP. (2021). *Becoming #GenerationRestoration: Ecosystem restoration for people, nature and climate* [Report]. U. N. E. Programme

University of Wyoming. (2025). Upper air soundings dataset [Dataset]. Retrieved from https://weather.uwyo.edu/upperair/sounding.html

Vancutsem, C., Ceccato, P., Dinku, T., & Connor, S. J. (2010). Evaluation of MODIS land surface temperature data to estimate air temperature in different ecosystems over Africa. *Remote Sensing of Environment*, *114*(2), 449–465. https://doi.org/10.1016/j.rse.2009.10.002

Veldman, J. W., Overbeck, G. E., Negreiros, D., Mahy, G., Le Stradic, S., Fernandes, G. W., et al. (2015). Where tree planting and forest expansion are bad for biodiversity and ecosystem services. *BioScience*, *65*(10), 1011–1018. https://doi.org/10.1093/biosci/biv118

Westra, D., Steeneveld, G. J., & Holtslag, A. A. M. (2012). Some observational evidence for dry soils supporting enhanced relative humidity at the convective boundary layer top. *Journal of Hydrometeorology*, *13*(4), 1347–1358. https://doi.org/10.1175/JHM-D-11-0136.1

Windisch, M. G., Davin, E. L., & Seneviratne, S. I. (2021). Prioritizing forestation based on biogeochemical and local biogeophysical impacts. *Nature Climate Change*, *11*(10), 867–871. https://doi.org/10.1038/s41558-021-01161-z

Wolfe, R. E., Lin, G., Nishihama, M., Tewari, K. P., Tilton, J. C., & Isaacman, A. R. (2013). Suomi NPP VIIRS prelaunch and on-orbit geometric calibration and characterization. *Journal of Geophysical Research: Atmospheres*, *118*(20), 11508–11521. https://doi.org/10.1002/jgrd.50873

Wolff, N. H., Masuda, Y. J., Meijaard, E., Wells, J. A., & Game, E. T. (2018). Impacts of tropical deforestation on local temperature and human well-being perceptions. *Global Environmental Change*, *52*, 181–189. https://doi.org/10.1016/j.gloenvcha.2018.07.004

Xie, D., Caporaso, L., Reichstein, M., Zhong, D., & Duveiller, G. (2025). Beyond canopy cover: How tree distribution shapes cloud formation across Africa [*Preprint*]. https://doi.org/10.21203/rs.3.rs-5639740/v1

Xu, R., Li, Y., Teuling, A. J., Zhao, L., Spracklen, D. V., Garcia-Carreras, L., et al. (2022). Contrasting impacts of forests on cloud cover based on satellite observations. *Nature Communications*, *13*(1), 670. https://doi.org/10.1038/s41467-022-28161-7

Zhang, Y., Wang, X., Lian, X., Li, S., Li, Y., Chen, C., & Piao, S. (2024). Asymmetric impacts of forest gain and loss on tropical land surface temperature. *Nature Geoscience*, *17*(5), 1–7. https://doi.org/10.1038/s41561-024-01423-3